3D SAR Imaging Using a Hybrid Decomposition Super-Resolution Technique

Walter S. Kuklinski[a], Andrea L. Kraay[a*]
[a]The MITRE Corporation, 202 Burlington Road, Bedford, MA 01730-1420

ABSTRACT

A technique to form super-resolved 3D Synthetic Aperture Radar (SAR) images from a limited number of elevation passes is presented in this paper. This technique models the environment as containing a finite number of isotropically radiating, frequency independent point scatterers in Additive White Gaussian Noise (AWGN), and applies a hybrid super-resolution method that yields the Maximum Likelihood (ML) estimates of scatterer strengths and resolves their locations in the data deficient dimension well beyond the Fourier resolution limit.

Keywords: Super-Resolution, SAR, Maximum Likelihood

1. INTRODUCTION

In most Synthetic Aperture Radar (SAR) applications, the available radar bandwidth and azimuthal aperture are sufficient to form high resolution 2D SAR images. Resolution in the third dimension, however, can be severely impaired by operational considerations that limit the available number of target to platform orientations. Modeling the environment as containing a finite number of isotropically radiating, frequency independent point scatterers in Additive White Gaussian Noise (AWGN), a hybrid super-resolution method is applied that yields the Maximum Likelihood (ML) estimates of scatterer strengths and resolves their locations in the data deficient dimension well beyond the Fourier resolution limit.

A series of 2D SAR images taken from different elevation passes is registered to yield samples of the limited frequency domain data at each 2D range/cross-range resolution cell. Processing is done on an individual 2D cell-by-cell basis to produce the super-resolved 3D SAR image. Using the above scattering model, a constrained gradient search is performed to minimize a mean square error (MSE) cost function to resolve scatterer locations and linearly estimate the scatterer strengths. In the case where the noise environment is accurately represented by AWGN, the linear estimator of scatterer strengths yields the ML estimates.

This technique is demonstrated with a simple 1D example and 3D XPATCH data.

2. THE DECOUPLED LEAST SQUARES TECHNIQUE

Here, a technique to super-resolve scatterers at a particular range and cross-range location in height out of the slant plane is presented. First, the environmental model and assumptions are set forth, then the approach to the nonlinear problem of resolving an unknown number of scatterers of unknown strengths and locations is described.

2.1 Environmental Model

It is assumed that at a particular range and cross-range point there are a finite number of isotropically radiating, frequency independent point scatterers dispersed spatially in height out of the slant plane. With the range/cross-range notation suppressed, the frequency domain data model at a range/cross-range cell may be written as:

$$S(\omega_z) = \sum_{k=1}^{K} a_k^* e^{-j\omega_z z_k} = \mathbf{a}^H \mathbf{v}(\omega_z) = \mathbf{v}^H(\omega_z)\mathbf{a} \tag{1}$$

*akraay@mitre.org; phone 1 781 271 2065; fax 1 781 271 7045; mitre.org

where z is the dimension of height out of the slant plane, ω_z is spatial frequency in (rad/m), a_z is the complex scattering amplitude of the k^{th} scatterer, z_k is the location of the k^{th} scatterer, "*" denotes scalar complex conjugation, and "H" denotes the vector Hermetian operator.

The unknown parameters to estimate are the number of scatterers, K, the scatterer strengths $\mathbf{a} = \{a_1, \ldots, a_K\}$, and their locations $\mathbf{z} = \{z_1, \ldots, z_K\}$, such that the model matches the available data samples at $\omega_z = \{\omega_{z1}, \omega_{z2}, \ldots, \omega_{zM}\}$, in a least squares sense. i.e.,

$$C = E\left[\left|S(\omega_z) - \hat{S}(\omega_z)\right|^2\right] \tag{2}$$

is minimized.

A direct approach to solve this problem would be to jointly estimate these parameters using a gradient-based search method. But because the minimization of this multi-dimensional cost function is a highly nonlinear problem, these techniques can be very unstable and are prone to converging on incorrect solutions at local extremma of the cost function.

More common approaches estimate the contributions from the individual scatterers one at a time and subtract them from the data in an iterative fashion. Examples of such deconvolution techniques are the CLEAN and RELAX algorithms.

Although these techniques can yield useful results, they do not always perform well when the point spread function does not accurately represent the scattering phenomena taking place. The sensitivities of these methods to the choice of point spread function motivate the development of a more robust technique to estimate the scatterer amplitudes and locations. We attempt to simplify the problem by decoupling the scatterer strengths with their locations, and establishing a hybrid (linear and non-linear) formulation.

2.2 Decoupled Least Squares Estimation

In this section, a technique to super-resolve scatterers at a particular range and cross-range location in height out of the slant plane is described. Building on the model and previously stated assumptions, the nonlinear problem is simplified by decoupling the scatterer strengths from their locations to solve a simpler series of hybrid (linear and non-linear) problems.

One approach to this problem is to assume a large number of scatterers, K, and use a finely spaced grid of allowable scatterer locations. This allows the vectors $\mathbf{v}(\omega_{z1})$, $\mathbf{v}(\omega_{z2})$, …$\mathbf{v}(\omega_{zK})$ to be used as known quantities, and the estimation of scatterer amplitudes at these locations becomes a linear problem.

Modeling the frequency domain data samples as:

$$\begin{bmatrix} y(\omega_{z1}) \\ y(\omega_{z2}) \\ \vdots \\ y(\omega_{zM}) \end{bmatrix} = \begin{bmatrix} \mathbf{v}^H(\omega_{z1}) \\ \mathbf{v}^H(\omega_{z2}) \\ \\ \mathbf{v}^H(\omega_{zM}) \end{bmatrix} \mathbf{a} + \mathbf{n} \tag{3}$$

$$\mathbf{y} = \mathbf{V}^H \mathbf{a} + \mathbf{n}$$

where $\mathbf{n}$ is a zero-mean complex Gaussian random vector with uncorrelated components, the maximum likelihood estimate of the complex scatterer amplitudes is:

$$\hat{\mathbf{a}}_{ML} = \left(\mathbf{V}\mathbf{V}^H\right)^{-1}\mathbf{V}\mathbf{y} \tag{4}$$

The limitation of this approach is that for a grid of many finely spaced scatterers, the matrix $\mathbf{V}\mathbf{V}^H$ may not have full rank and be invertible.

The Decoupled Non-Linear Least-Squares Estimation assumes that K is a small number (on the order of, say, 5) and assumes the locations of the K scatterers are confined to a finely spaced grid in z, with a specified minimum separation between them. For each possible combination of K unique scatterer locations, the amplitudes, $\hat{\mathbf{a}}_{ML}$, are computed and the mean square error between the model and the available data is evaluated. After evaluating this exhaustive set of possible solutions, the scatterer configuration and respective amplitude estimates that yield the minimum mean square error are chosen as the final solution.

A block diagram of the decoupled non-linear least-squares estimation procedure is shown below in Figure 1. The implementation details are provided in Appendix A.

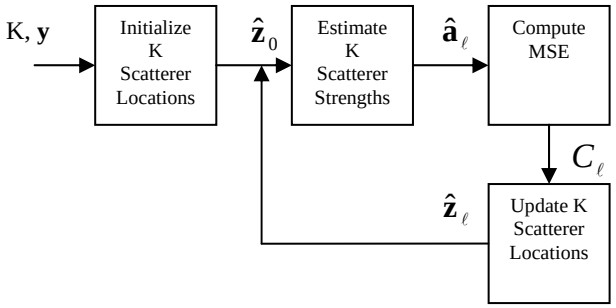

Figure 1. Decoupled Least Squares Estimation Procedure

3. NUMERICAL RESULTS

The performance of the Decoupled Non-Linear Least Squares estimation procedure has been demonstrated with a simple 1D example and with 3D XPATCH data.

1D Example

The technique is demonstrating using a simple 1D example with received data that matches the model exactly.

Consider a case where a 5-meter region in *z* is to be imaged and 10 frequency samples spaced at $\Delta\omega_z = 2\pi/5$ (rad/m) are given, yielding a Fourier spatial resolution of $\Delta z = 0.5$m. The environment consists of 4 point scatterers in white Gaussian noise at locations $\mathbf{z} = \{2.0\text{m}, 2.4\text{m}, 3.5\text{m}, 4.25\text{m}\}$ and with corresponding amplitudes $\mathbf{a} = \{10, 10, 0.5, 7\}$. The noise samples are zero-mean complex Gaussian and uncorrelated with variance $\sigma^2 = 1$. The true scene is depicted in Figure 2.

The data is processed assuming that the number of scatterers is K = 3. The Decoupled -Linear Least Squares estimation procedure is applied to the data according to the details provided in the Appendix. The scatterer locations were initialized to be the K Inverse Discrete Fourier Transform (IDFT) bins that contained the strongest amplitude estimates (bin sizes were chosen to be equal to the data's 0.5-m spatial resolution): $\mathbf{z}_0 = \{2.0\text{m}, 2.5\text{m}, 4.5\text{m}\}$. A 64-point IDFT of the data is shown in Figure 3 for reference along with the initial scatterer location estimates.

The minimum spacing of scatterers was chosen to be 0.125m which is one-quarter the Fourier resolution. As can be seen in the 64-point IDFT of Figure 3, the two closely spaced scatterers are indistinguishable from one another due to the lack of sample support.

Figure 4 (top) shows the estimated scene as a result of an exhaustive search of the cost function. The scatterer location estimates are near their true values, but contain errors. This is due to the finite scatterer grid spacing of 0.125m of on which the search was performed. The MSE cost function is plotted versus scatterer configuration index in Figure 5, and the detected minimum is highlighted by the dashed line. When plotted against the single dimension of scatterer

configuration index, the cost function is multi-modal and nearly impossible to minimize using conventional gradient based search methods. When plotted against the K separate dimensions of the individual scatterer locations as in Figure 6, we see the cost function has a clear global minimum without nearby extremma. Figure 7 depicts the cost function of Figure 6 with the minimum exposed. This cost function structure suggests we may be able to use a gradient descent algorithm to update the scatterer location estimates and reduce the number of cost function evaluations.

Figure 4 (bottom) shows the scene estimate as a result of the gradient-based search of the cost function. In this particular example, the scatterer location estimates for the gradient search method also contain a small amount of error. Sources of error may include imperfect function minimization and overestimation of minimum scatterer separation.

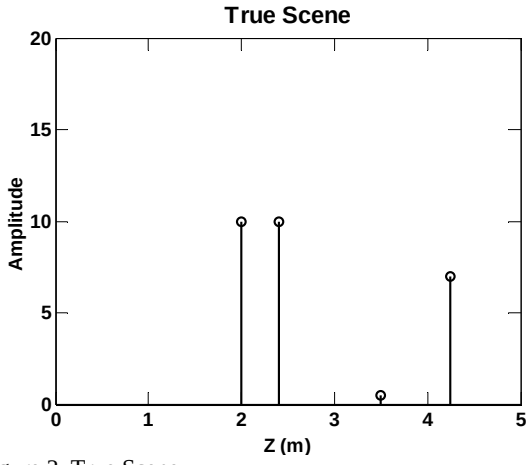

Figure 2. True Scene

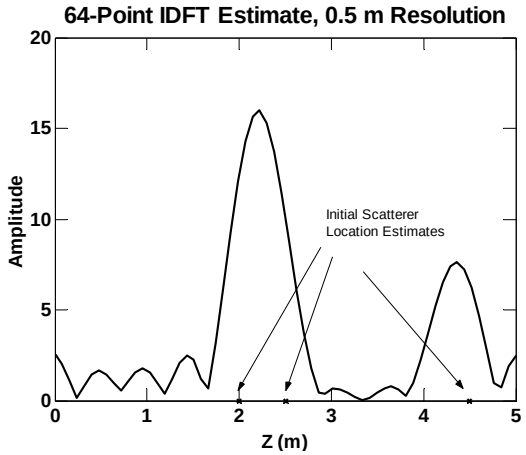

Figure 3. 64-Point IDFT Estimate of Scene

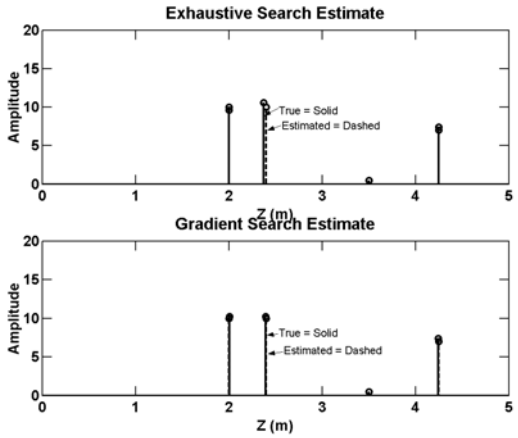

Figure 4. Scene Estimates. (top) Exhaustive (bot) Gradient

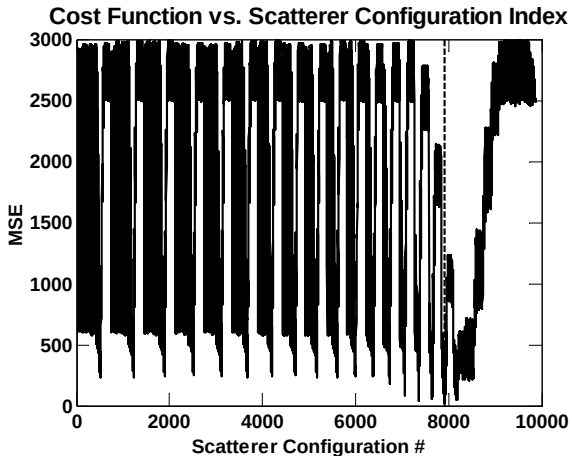

Figure 5. MSE Cost Function vs. Scatterer Configuration Index. Dashed Line Represents Location of Minimum

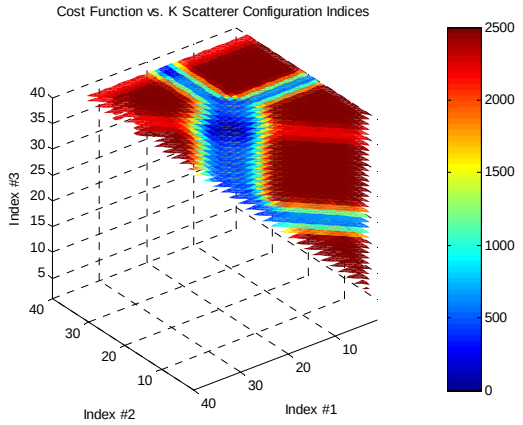

Figure 6. MSE Cost Function vs. Individual Scatterer Locations

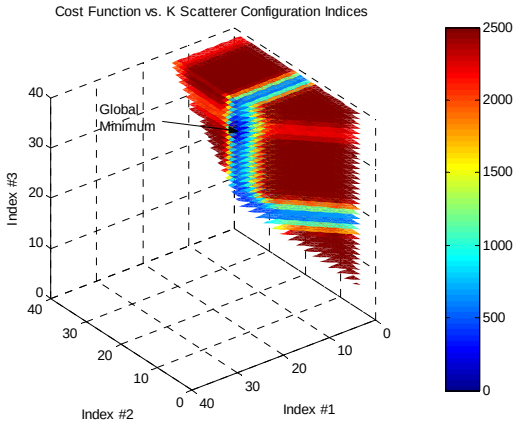

Figure 7. MSE Cost Function w/ Exposed Minimum

3.2 Processing 3D XPATCH Data

The Decoupled Least-Squares technique was tested on simulated SAR data of an M113 Troop Carrier generated using XPATCH and compared to the output of a 64-point IDFT.

3.2.1 Data Collection

The radar center frequency and bandwidth were 10.0 GHz and 2.95 GHz, respectively. The video phase history was collected for 9 evenly spaced elevation passes between 28° and 30° at an azimuth of 20° and infinite standoff range, as depicted in Figure 8. Each elevation pass yields a 256x256-pixel SAR image sampled at twice the 2" (5.08cm) resolution in range and cross-range using HH polarization.

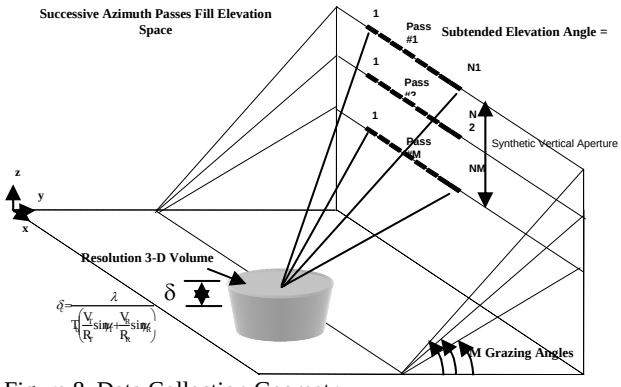

Figure 8. Data Collection Geometry

3.2.2 Data Format & Pre-Processing

In order to use the same processing in ω_z that was employed in the previous example, the available frequency domain data needs to be put into the proper format. This is done by first transforming the collected data into the orthogonal dimensions of range, cross range and ω_z, and then processing in ω_z on range cell-by-cross range cell basis.

The available frequency domain data falls onto a spherical raster as highlighted in Figure 9. The dimensions (x', y', z') $\leftrightarrow$ (ω_x',ω_y',ω_z') represent a coordinate system rotated relative to the reference Cartesian system used in the data collection. For simplicity, we perform our processing in the rotated and shifted (x,y,z) $\leftrightarrow$ (ω_x,ω_y,ω_z) coordinate system, where (x,y,z) correspond to the dimensions of range, cross-range, and height out of slant plane, respectively.

To transform the data into the dimensions of (x,y,ω_z), a two-step process is followed: First we form a set of high-resolution 2D SAR images from the data taken at each elevation pass[1]. We subsequently interpolate these images to points in the common (x,y,ω_z) coordinate system as shown in Figure 10. The individual 2D SAR images are provided in the Appendix for reference. Note that sample spacing in ω_z is a function of the range cell being processed, as well as the length of the region we may image in z and the Fourier resolution. These are given by:

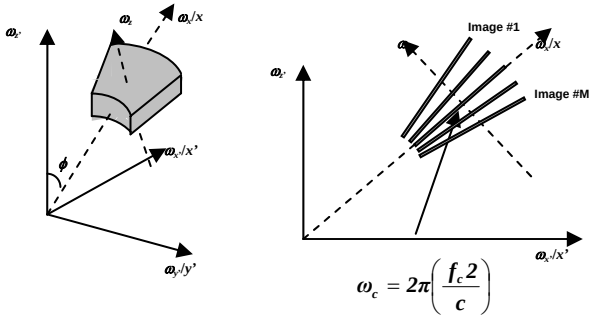

Figure 9. Frequency Domain Data Format

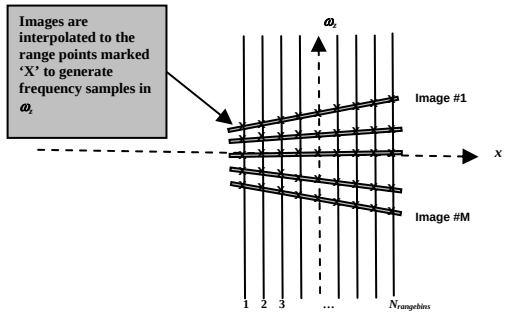

Figure 10. Data Interpolation Scheme

$$d\omega_z(i) = 2\pi \frac{2}{c}\left(f_c + \frac{BW}{N_{rangebins}}\left(i - \frac{\left(N_{rangebins} - 1\right)}{2}\right)\right)\frac{\left(\tan\left(\phi_o - \phi_{\min}\right) - \tan\left(\phi_o - \phi_{\max}\right)\right)}{M} \tag{5}$$

$$L_z(i) = \frac{2\pi}{d\omega_z(i)} \tag{6}$$

$$\Delta z_{Fourier}(i) = \frac{L_z(i)}{M} \tag{7}$$

where

i	Index of the range bin being processed and increases with range from the radar, $0 \le i \le N_{rangebins}$-1
$N_{rangebins}$	Total number of range bins being processed
c	Speed of light (m/s)
f_c	Radar center frequency (Hz)
BW	Radar bandwidth (Hz)
M	Number of elevation passes

1 Complex SAR Images were formed at individual elevation passes by interpolating the data from a polar to a Cartesian raster, applying a 2D Kaiser window for sidelobe reduction and performing an Inverse Fast Fourier Transform (IFFT). Kaiser windows with peak sidelobe levels of -40 dB were used and the images were (256x256) in size sampled at 2x the Nyquist Rate.

ϕ_o	Mean elevation angle of passes (rad)
ϕ_{min}	Minimum elevation angle of passes (rad)
ϕ_{max}	Maximum elevation angle of passes (rad)
$L_z(i)$	Length of the unambiguous region that may be imaged in z at the i^{th} range bin (m)
$\Delta z_{Fourier}(i)$	Fourier resolution in z at the i^{th} range bin (m)

3.2.3 Data Processing

Once the frequency domain data has been placed in the appropriate coordinate system as described above, we then use the gradient-based decoupled least squares technique at each range/cross-range index. Additionally, we incorporate scatterer location constraints as a function of range. The scatterer locations estimates are constrained to lie between the ground and a distance $L_z(i)$ above the ground. Figure 11 illustrates the change in ground plane location as a function of range.

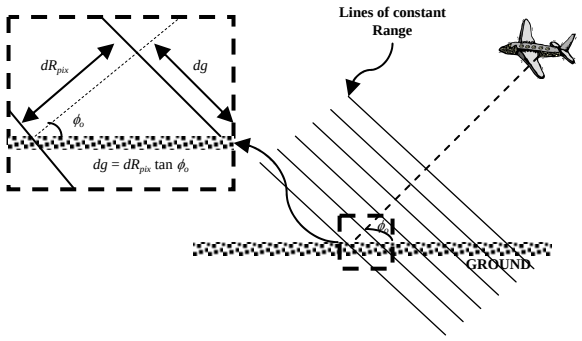

Figure 11. Ground Location as a Function of Range

The minimum and maximum value for a scatterer location in z at the i^{th} range bin may be expressed as:

$$z_{\min}(i) = \left(i - \frac{N_{rangebins} - 1}{2} \right) \cdot dR_{pix} \tan\phi_o \tag{8}$$

$$z_{\max}(i) = z_{\min}(i) + L_z(i) \tag{9}$$

where

I	Index of the range bin being processed and increases with range from the radar, $0 \le i \le N_{rangebins}$-1
$N_{rangebins}$	Total number of range bins being processed
dR_{pix}	Range resolution per pixel (m)
ϕ_o	Mean elevation angle of passes (rad)
$L_z(i)$	Length of the unambiguous region that may be imaged in z at the i^{th} range bin (m)

In processing the XPATCH data, the number of scatterers was assumed to be K = 3, and we apply the Decoupled - Linear Least Squares estimation processing according to the details provided in the Appendix. As before, the scatterer locations are initialized to be the K Inverse Discrete Fourier Transform (IDFT) bins that contained the strongest amplitude estimates. Bin sizes are chosen to be equal to the data's Fourier resolution at the range cell being processed, $\Delta z_{Fourier}(i)$. The minimum scatterer spacing constraint is set to be one-quarter the Fourier resolution.

3.2.4 Results

Figures 12-17 show the 3D SAR images of the DLS technique and direct Fourier inversion overlaid with the CAD model. The vertical smearing normally present in the Fourier-inversion image has been suppressed by picking the peak value of a 64-point IDFT at each range/cross-range cell. Points that capture 75% of the total energy in the images are displayed.

The DLS image contains more spurious points than the (modified) Fourier-inversion image, but highlights the important features of the troop carrier, with more points concentrated around most scattering centers.

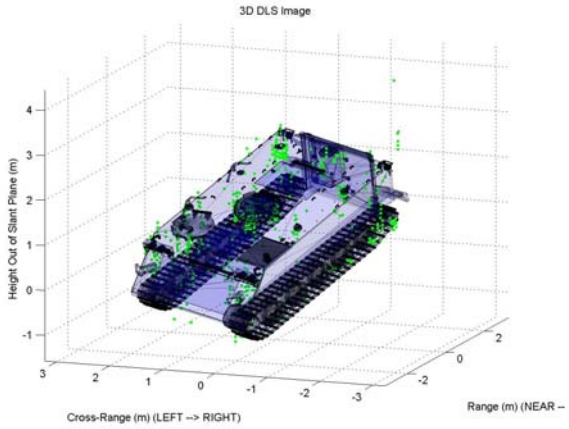

Figure 12. DLS Estimates w/ CAD Model, General View

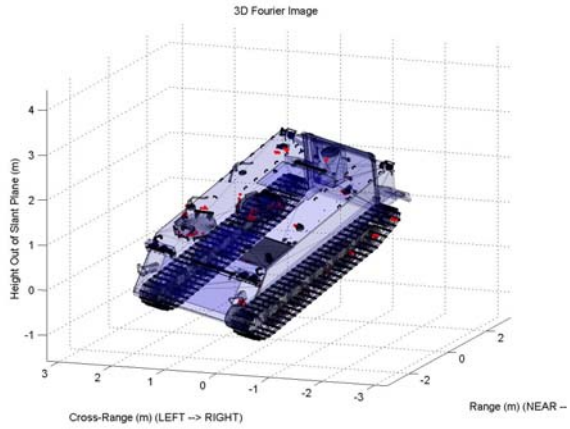

Figure 13. Fourier Estimates w/ CAD Model, General View

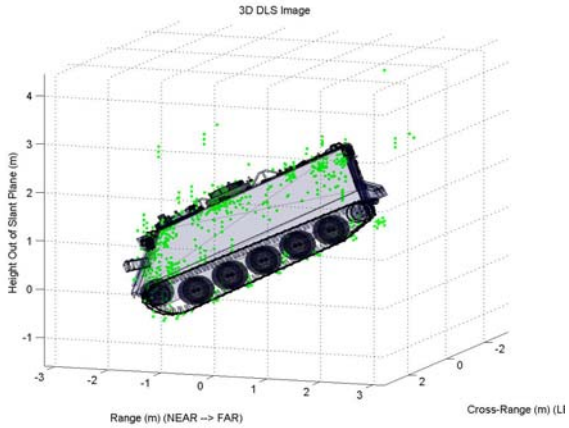

Figure 14. DLS Estimates w/ CAD Model, Left Side View

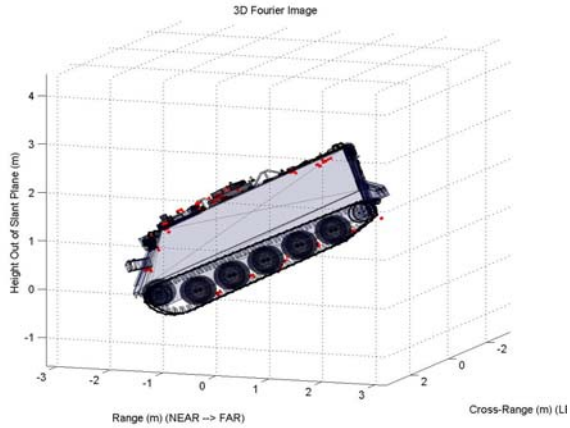

Figure 15. Fourier Estimates w/ CAD Model, Left Side View

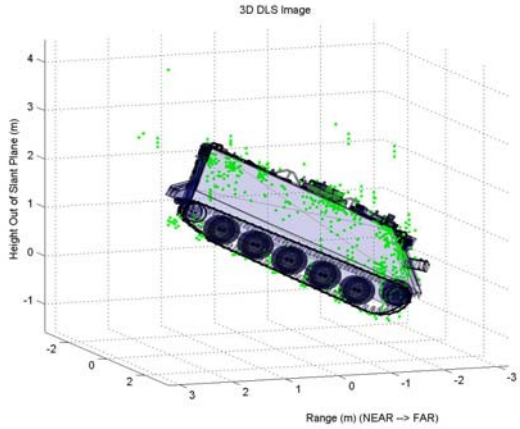

Figure 16. DLS Estimates w/ CAD Model, Right Side View

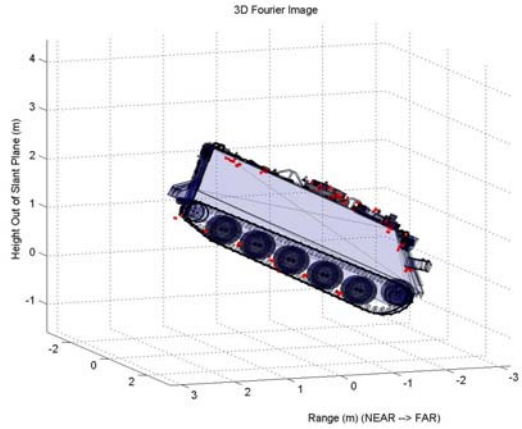

Figure 17. Fourier Estimates w/ CAD Model, Right Side View

SUMMARY

High-quality 3D SAR image formation can be severely impaired by operational considerations that limit the available number of target to platform orientations. The Decoupled Least Squares (DLS) technique to form super-resolved 3D SAR images from a limited number of elevation passes has been presented in this paper.

In the ideal case where there is no or little data and model mismatch, the DLS technique resolves point scatterers well beyond the Fourier resolution limit. In a more realistic environment, the DLS technique appears to highlight key object features better than (modified) Fourier-inversion, but in some cases yields spurious points as well.

Topics for future consideration are comparison of the DLS technique to compare to CLEAN and RELAX algorithms, and incorporation of more accurate scattering models.

APPENDIX A: IMPLEMENTATION DETAILS FOR DECOUPLED LEAST-SQUARES ESTIMATION

The Decoupled Non-Linear Least Squares Estimation procedure has four main stages of processing, as shown in Figure 1: i) Initialization of scatterer locations; ii) Scatterer strength estimation; iii) MSE computation; and iv) Update of scatterer location. The implementation of these stages for the examples presented in this document is described here.

A.1 Scatterer Location Initialization

The scatterer locations are initialized to be the bin centers (at the Fourier resolution) of the K largest IDFT values. For example, if we have N frequency domain samples of data with a known Fourier spatial resolution of *dz* meters, we choose the z_b for the K largest values of:

$$\left|s_{IDFT}\left(z_b\right)\right| = \left|\frac{1}{N}\sum_{n=0}^{N-1} S\left(\omega_{z,n}\right) e^{j\omega_{z,n} z_b}\right| \tag{A.1}$$

where the bin center $z_b = z_i + b \cdot dz$, b = 0,…,N-1, and $\{S(\omega_{z,0}), S(\omega_{z,1}), \ldots, S(\omega_{z,N-1})\}$ are the N samples of frequency domain data.

A.2 Scatterer Strength Estimation

Building on the environmental model and notation defined in equations (1) and (3), we assume that the data may be modeled as:

$$\mathbf{y} = \mathbf{V}^H \mathbf{a} + \mathbf{n} \tag{A.2}$$

where **n** is a zero-mean complex Gaussian random vector with uncorrelated components, and **V** is constructed from our known frequency sample points and our K estimated scatterer locations. We then use maximum likelihood estimator for the complex scatterer amplitudes:

$$\hat{\mathbf{a}}_{ML} = \left(\mathbf{V}\mathbf{V}^H\right)^{-1}\mathbf{V}\mathbf{y} \tag{A.3}$$

A.3 MSE Computation

The MSE between our current model and the data is computed as:

$$\begin{aligned} MSE &= E\left[\left|S\left(\omega_z\right) - \hat{S}\left(\omega_z\right)\right|^2\right] \\ &= \left(\mathbf{y} - \mathbf{V}_\ell^H \hat{\mathbf{a}}_\ell\right)^H \left(\mathbf{y} - \mathbf{V}_\ell^H \hat{\mathbf{a}}_\ell\right) \end{aligned} \tag{A.4}$$

where **y** is the frequency domain data, $\mathbf{V}_\ell^H$ is constructed from our known frequency sample points and our K current estimated scatterer locations, and $\hat{\mathbf{a}}_\ell$ contains our K current estimates of the complex scatterer amplitudes.

A.4 Scatterer Location Estimation

The scatterer location estimates are updated using a constrained cost function minimization technique from MATLAB®'s Optimization Toolbox called `fmincon`. The technique uses a Sequential Quadratic Programming (SQP)

method that forms a quadratic approximation to the Lagrangian function. Our constraints were chosen such that all scatterers lie within the region in z that we are imaging (of length L_z), and $z_1 + \varepsilon < z_2$, $z_2 + \varepsilon < z_3$, …, $z_{K-1} + \varepsilon < z_K$, where ε is a minimum scatterer separation. Figure A-1 depicts the three major steps per iteration of the algorithm.

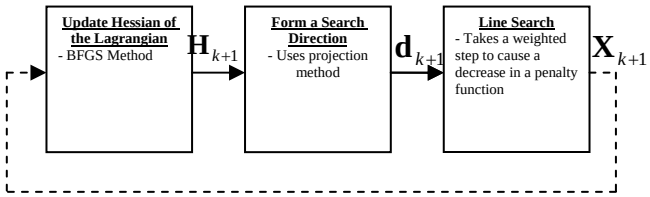

Figure A-1. Cost Function Minimization

APPENDIX B: ELEVATION PASS 2D SAR IMAGES

The SAR images formed from data taken at the individual elevation passes are presented in Figures B-1 and B-2. The images shown represent the magnitude of the complex SAR data.

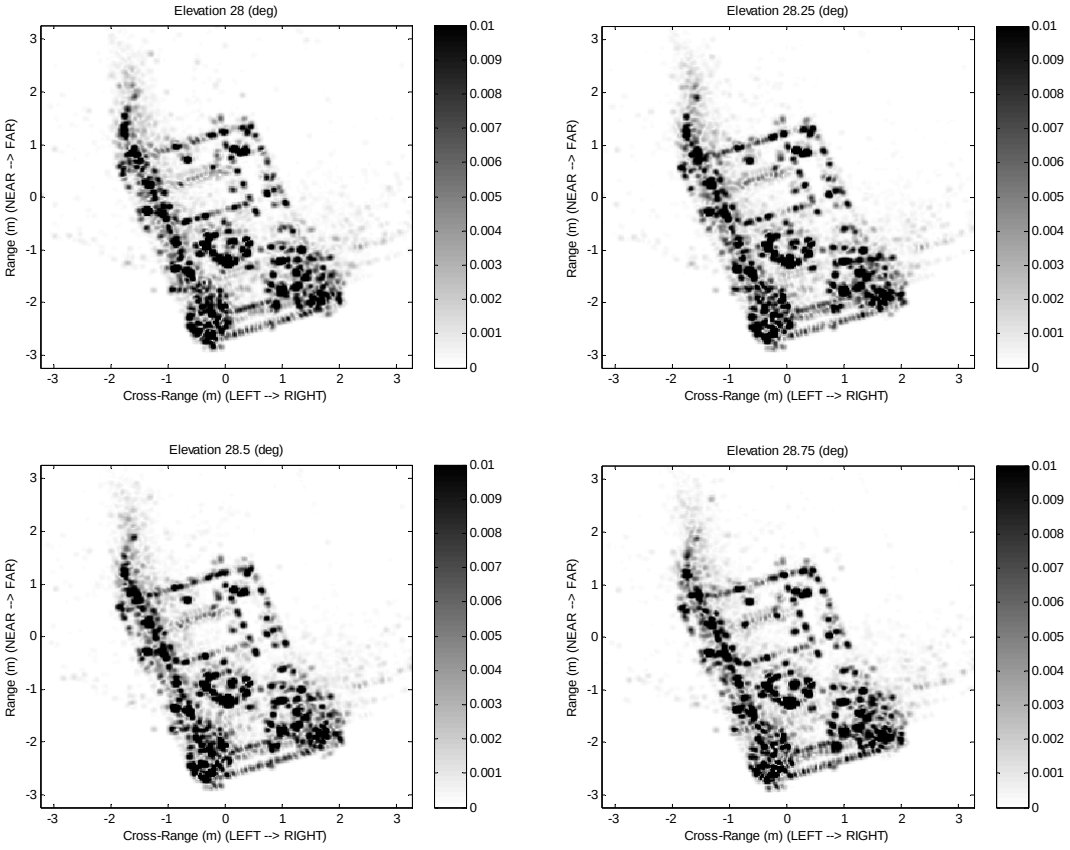

Figure B-1. 2D SAR Images from Elevation Passes $\phi = 28^o$-28.75^o

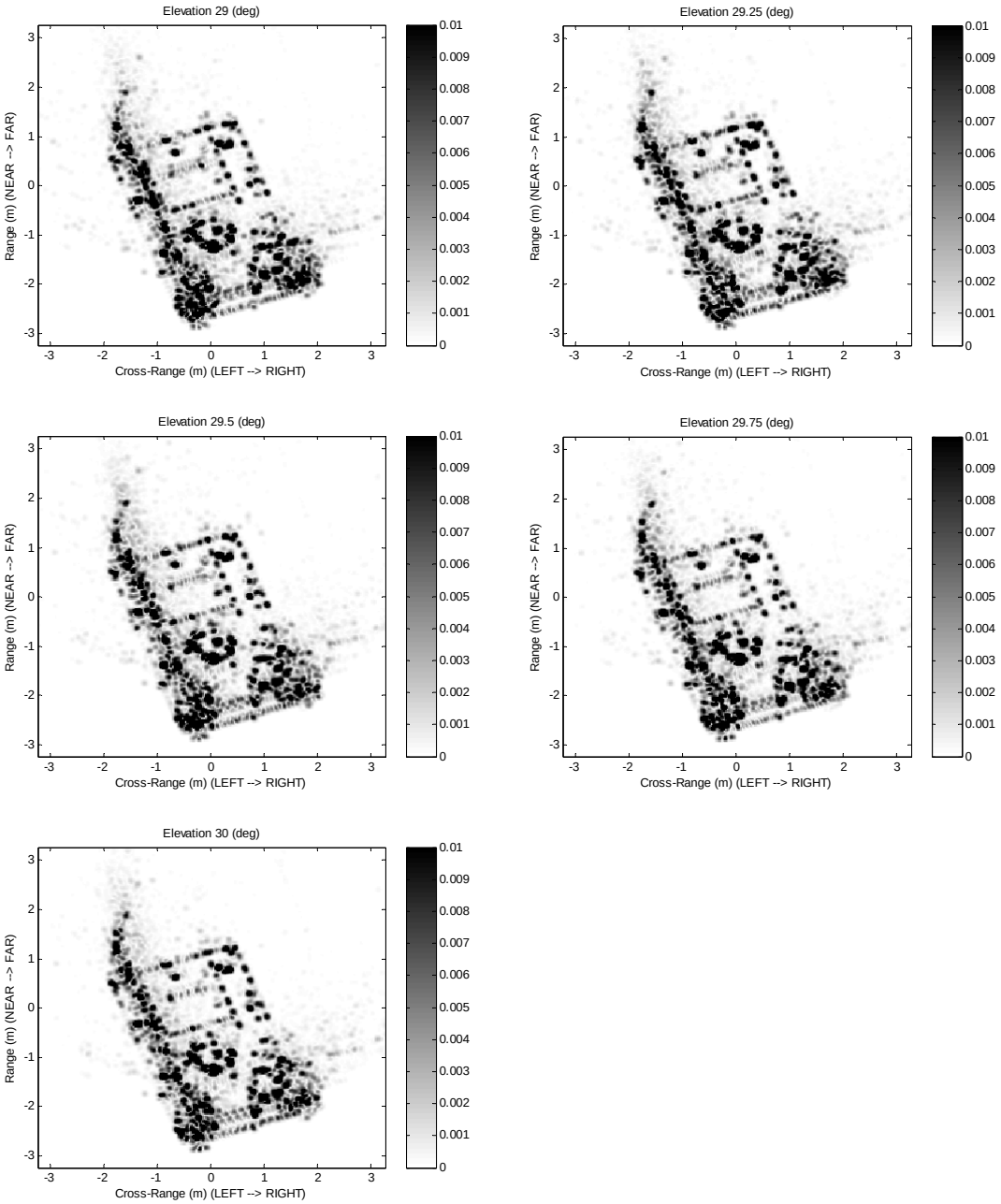

Figure B-2. 2D SAR Images from Elevation Passes $\phi = 29^{o}$-30^{o}

REFERENCES

1. M.W. Castelloe, D.C. Munson, "3-D SAR Imaging via High-Resolution Spectral Estimation Methods: Experiments with XPATCH", *IEEE Proceedings of the International Conference on Image Processing*, **Vol. 1**, pp 853-856, 1997.
2. M.D. Desai, W.K. Jenkins, "Convolution Backprojection Image Reconstruction for Spotlight Mode Synthetic Aperture Radar", IEEE *Transactions on Image Processing*, **Vol. 1**, pp 505-517,1992.
3. M.J. Gerry, et. al., "A Parametric Model for Synthetic Aperture Radar Measurements", *IEEE Transactions on Antennas and Propagation*, **Vol. 47**, pp 1179-1188, 1999.
4. J. Li, et. al., "A Robust Semi-Parametric Method for Feature Extraction and SAR Image Formation of Targets Consisting of Trihedrals and Dihedrals", *SPIE Conference on Algorithms for Synthetic Aperture Radar Imagery VI*, **Vol. 3721**, pp 92-103, 1999.